

NASA Technical Memorandum 89833

Performance and Efficiency Evaluation and Heat Release Study of an Outboard Marine Corporation Rotary Combustion Engine

(NASA-TM-89833) PERFORMANCE AND EFFICIENCY
EVALUATION AND HEAT RELEASE STUDY OF AN
OUTBOARD MARINE CORPORATION ROTARY
COMBUSTION ENGINE (NASA) 24 F CSCI 21A

N87-20282

Unclas
G3/07 45386

H.L. Nguyen, H.E. Addy, T.H. Bond,
C.M. Lee, and K.S. Chun
Lewis Research Center
Cleveland, Ohio

Prepared for the
1987 International Congress and Exposition
sponsored by the Society of Automotive Engineers
Detroit, Michigan, February 23-27, 1987

NASA

PERFORMANCE AND EFFICIENCY EVALUATION AND HEAT RELEASE STUDY OF AN
OUTBOARD MARINE CORPORATION ROTARY COMBUSTION ENGINE

H.L. Nguyen, H.E. Addy, T.H. Bond, C.M. Lee, and
K.S. Chun

National Aeronautics and Space Administration
Lewis Research Center
Cleveland, Ohio 44135

SUMMARY

A computer simulation which models engine performance of Direct Injection Stratified Charge (DISC) rotary engines has been used to study the effect of variations in engine design and operating parameters on engine performance and efficiency of an experimental Outboard Marine Corporation (OMC) rotary combustion engine. Engine pressure data have been used in a heat release analysis to study the effects of heat transfer, leakage and crevice flows. Predicted engine data is compared with experimental test data over a range of engine speeds and loads. An examination of methods to improve the performance of the rotary engine using advanced heat engine concepts such as faster combustion, reduced leakage and turbocharging is also presented.

INTRODUCTION

The direct-injection stratified-charge (DISC) Wankel rotary engine is currently being evaluated by NASA as a future advanced powerplant for light commercial and similar applications. The Wankel rotary engine offers attractive advantages over the reciprocating engines for use in small aircraft. These advantages include higher power to weight ratio, simpler and more compact shape, fewer moving parts, lower noise levels and less vibration. In addition, using direct-injection stratified-charge operation, the rotary engine can be designed for operation with jet-fuel or multi-fuel capability (refs. 1 and 2).

The purpose of this study is to examine the combustion rate and performance loss mechanisms of an experimental Outboard Marine Corporation (OMC) DISC Wankel rotary engine. The test program was conducted using an OMC single rotor experimental engine at NASA Lewis Research Center to obtain engine performance data and to investigate the stratified-charge concept. To support these testing activities, numerical simulations were used to examine heat release and heat loss mechanisms (such as heat transfer, crevice volumes and gas leakage). These simulations were also used to investigate how DISC Wankel engine performance varies with changes in engine design and operating conditions. Experimental pressure data obtained from the OMC rotary test engine were used with the heat release rate computer model to compute the fuel burning rate and loss mechanisms. Performance predictions of the OMC engine were compared with experimental data. The performance improvements of the DISC Wankel rotary engine were also investigated.

MODELS DESCRIPTION REVIEW

Two thermodynamic simulation models were used to predict the performance of DISC Wankel rotary engines. These models were developed by researchers at Sloan Automotive Laboratory, Massachusetts Institute of Technology (ref. 3). The first type of computer model may be used to determine the combustion heat release rate from measured chamber pressure using a heat release analysis based on a first-law thermodynamic analysis on the contents of the engine combustion chamber. The combustion chamber is treated as an open thermodynamic system, and its contents are effectively modeled as uniform and homogeneous. Thermodynamic properties of the chamber contents are represented by a simple linear function of temperature for the ratio of specific heats γ (ref. 4). The fuel chemical energy released inside the combustion chamber is accounted for by all the major energy and mass transport mechanisms: heat transfer, leakage and crevice volume effects. In performing the heat transfer calculation, the convective heat transfer to combustion chamber walls is calculated in addition to the heat transfers associated with flow into and out of crevices. Heat transfer due to flows through leakage paths is also simulated. The forced convective heat transfer is based on the form proposed by Woschni (ref. 5). The heat transfer coefficient appearing in the Woschni equation takes the following form:

$$h = 131.0 R^{-0.2} P^{0.8} T^{-0.53} W^{0.8} \quad (1)$$

where R is the rotor radius, P is the chamber pressure, T is the chamber average temperature, and W is the characteristic speed given by:

$$W = 2.28 C_1 U_R + 0.324 C_2 \left(\frac{V_{disp}}{V_{IPC}} \right) \left(\frac{P_f - P_m}{P_{IPC}} \right) T_{IPC} \quad (2)$$

U_R is the mean rotor speed, V is the chamber volume, the subscript IPC refers to conditions at intake port closing, p_f and p_m are firing and motoring pressures, respectively, and V_{disp} is the displacement volume. C_1 and C_2 are scaling coefficients and are adjusted according to the calibration procedure described in the following section. Crevice and leakage phenomena are combined, i.e., the leakage flow path to an adjacent chamber is assumed to occur via a crevice region.

To assist in formulating the combustion model, a single empirical model which defines the rate of heat release for a range of speeds and loads was used (ref. 3). From the start of combustion at crank angle θ_s , the heat release rate rises linearly to $(dQ/d\theta)_m$, the peak rate of heat release, which occurs at θ_m , the crank angle position at peak rate of heat release. The heat release rate then decays exponentially with a time constant, τ , until the exhaust port begins to open. An integral constraint defines the sum of the integrated heat release rates between the intervals θ_s to θ_m , and θ_m to exhaust port opening, as the combustion efficiency, η_{comb} , times the energy of the injected fuel. This integral constraint was used to aid in computing the four parameters appearing in the heat release empirical model. Therefore, only three of the four model parameters need be specified with the fourth being determined by the constraint. From θ_s to θ_m , the rate of heat release is given by:

$$\frac{dQ}{d\theta} = \left(\frac{dQ}{d\theta} \right)_m [(\theta - \theta_s) / (\theta_m - \theta_s)] \quad (3)$$

For a crank angle greater than the peak rate location θ_m , the rate of heat release is given by:

$$\frac{dQ}{d\theta} = \left(\frac{dQ}{d\theta} \right)_m \exp [(\theta - \theta_m) / \tau] \quad (4)$$

with, τ , as the fourth value given by the integral constraint:

$$\tau = \left\{ \left[n_{\text{comb}} \left(\frac{dQ}{d\theta} \right)_m \right] - \frac{1}{2} (\theta - \theta_s) \right\} \quad (5)$$

The above heat release model can provide both a useful check on the quality of measured chamber pressure data, and an accurate method for predicting combustion rates from measured chamber pressure data.

The second numerical simulation model has been used to predict the development of the chamber pressure with time, and thereby the engine performance, from a prespecified combustion rate. The engine simulation model divides the complete engine cycle into the following periods: intake, compression, combustion (and expansion), and exhaust. The engine simulation is based on a first-law thermodynamics analysis of the engine combustion chamber with the following major assumptions:

(1) Quasi steady one-dimensional compressible flow equations are used to calculate the mass flows through the ports.

(2) The intake and exhaust manifolds are treated as infinite plenums with specified pressure and temperature histories.

(3) A one-zone combustion model in which the combustion rate is specified by a heat release rate equation is used. This one-zone model describes the chamber contents by a time-varying average overall equivalence ratio and temperature.

(4) Heat transfer to rotor and housings is modeled as turbulent convection over a flat plate where the corresponding Nusselt-Reynolds number correlation is used. Also, heat transfer to crevice walls is based on crevice gas properties evaluated at the crevice wall temperature. Radiative heat transfer is neglected.

(5) Crevices are modeled as containing gas at chamber pressure and wall temperature.

(6) Leakage occurs from a crevice region to an adjacent chamber (at lower pressure). One-dimensional quasi-steady compressible flow equations are used to model leakage flows.

(7) Thermodynamic properties (enthalpy and density) of the chamber contents are specified as functions of chamber temperature, pressure and average equivalence ratio. The ideal gas law is obeyed throughout the cycle.

The heat release rate and the engine simulation programs can be used as diagnostic tools to predict the performance of DISC Wankel engines when changes in the engine design and operating conditions are made.

MODEL CALIBRATION AND VALIDATION METHODOLOGIES

Prior to calibration and validation of the programs, a test of the heat release program was carried out. The engine simulation program was used to obtain the chamber pressure during a complete engine cycle. For this simulation the average speed of the engine was 3200 rpm and the equivalence ratio, $\phi = 0.39$. Details of the engine geometry and operating conditions are given in the next section. The heat release rate profile used as input for this simulation is shown in figure 1(b). As described in the previous section, this heat release rate model rises linearly from the start of combustion, at θ_s , to the peak rate of heat release, $(dQ/d\theta)_m$, which occurs at θ_m . The heat release rate then decays exponentially, with time constant, τ . The chosen model parameter values were: $\theta_s = 25.0^\circ$ BTC, $\theta_m = 0^\circ$ TDC, $(dQ/d\theta)_m = 0.0381$ (1/deg), and $\tau = 38.484^\circ$. The pressure curve generated from the engine simulation shown in figure 1(a) was then used as input to the heat release program. Both the engine simulation and heat release rate programs use similar values for wall temperatures and for the parameters in the submodels for heat transfer, and crevice volume and leakage area. The rate of heat release was then predicted from the heat release analysis and is compared to the original heat release rate model in figure 1(b). The heat release rate profiles are identical except for a small difference in the exponential decay. It was therefore decided that the heat release program was functioning properly.

The calibration and validation strategies of the heat release and engine simulation programs are discussed next. The heat release program and the engine cycle simulation involve a number of submodels containing empirical constants which require calibration against experimental data. For example, the following values of empirical constants in various submodels must be specified: the two scaling factors in the heat transfer model, the values for the crevice volume and the leakage area, the wall temperature, the ratio of specific heats, and the values of the discharge coefficients. Experimental data obtained from the motoring and firing OMC engine were used in the calibration and validation procedures. The calibration and validation procedures were the following:

(1) Experimental ensembled pressure traces versus crank angle data were used as input to the heat release program. As a starting point, estimates for the values of the heat transfer constants, crevice volume, leakage area, and discharge coefficients were used. Computations of the individual heat release rates and the integrated heat release (gross heat release) rates were performed. The gross heat release should be zero before start of combustion. At the end of combustion, the curve should be nearly flat with a value very close to the fuel energy (mass of fuel times its lower heating value per unit mass). Therefore, the gross heat release curves provide useful checks for the heat release model.

(2) From the individual heat release rates computed at varying speed and load points, an average heat release rate was calculated.

(3) The empirical heat release rate model was then fitted to the average calculated heat release rate. A set of four best-fitted parameters (θ_s , $(dQ/d\theta)_m$, θ_m , and τ) was obtained.

(4) The heat release rate obtained in the previous step was used as input to the engine simulation program. The predicted pressure traces were then compared against experimental ensemble averaged pressure traces. This iteration scheme was repeated until convergence between the computed and experimental ensembled pressure traces was obtained. This study was the baseline case where all the heat loss mechanisms were considered.

HEAT RELEASE PARAMETRIC ANALYSIS

In order to investigate the effects of heat transfer, crevice volume and leakage area on heat release and engine performance the following parametric study was performed.

(1) The fitted heat release rate from the baseline case was used as input to the engine simulation. Heat transfer was neglected. A corresponding pressure versus crank angle curve was obtained.

(2) The pressure data obtained in the previous step was used to calculate the corresponding heat release rate profile. This heat release rate profile was used in the fitting procedure to obtain four new best-fitted parameters in the empirical heat release rate model. This heat release rate model was then used in the engine simulation to compute a new pressure trace versus crank-angle. This new pressure trace was used as input to the heat release rate program to calculate the new heat release rate profile. This iteration scheme was repeated until consistency was achieved.

Steps 1 and 2 were repeated for additional cases where crevice volumes and leakage area were selectively neglected.

Since leakage area has a substantial effect on motoring pressure data at low speed, the estimated leakage area can be checked by running the engine simulation under motoring conditions. The computed motoring pressure traces were then compared to the experimental pressure traces. This procedure was followed and the estimated leakage area was adjusted until agreement between the calculated and experimental motoring pressure traces was achieved.

ROTARY ENGINE TEST RIG AND INSTRUMENTATION

Figure 2 shows the test rig which was constructed around a single rotor, 39.6 in.³ (0.648 liter) displacement, rotary engine built by the Outboard Marine Corporation (OMC). The engine is naturally aspirated and incorporates direct fuel injection combined with spark ignition to create a stratified-charge environment for combustion.

One fuel injector and one spark plug were used. Intake air is passed through the rotor to eliminate the need for an oil cooling system. Liquid coolant is directed peripherally around the hot side of the rotor housing to simplify the rotor and the side housing geometry. Figure 3 shows the path of the coolant through the engine.

The engine was designed to operate under a stratified-charge, overall fuellean condition similar to a direct-injection diesel engine. Air flow to the engine was not constricted or throttled. The flowpath along with the heating effect associated with cooling the rotor were found to adversely affect the volumetric efficiency.

The fuel system consisted of a distributor type injection pump (Stanadyne Model No. DB-2) and a four hole pencil injector (Stanadyne Model No. XNM-1753) which was located near the minor axis of the trochoid housing. The fuel used was an ASTM diesel check fuel with a cetane number of 53.7.

A single spark plug located on the minor axis of the trochoid housing was used to initiate combustion. A single spark per power stroke was generated by a capacitive discharge type ignition system.

Lubrication for the main bearings, rotor bearings, and the rotor seals was provided by two solenoid-operated metering pumps. The lubricating oil was a synthetic, two-cycle oil which was not recirculated, but was consumed in the combustion process. The heat of combustion of the oil was negligible in comparison to the total heat of combustion of the fuel.

The remainder of the test rig consisted primarily of an eddy current dynamometer and an electric motor. The motor was capable of motoring the engine up to speeds of 3200 rpm, while the dynamometer could absorb engine torques up to 50 ft-lb, at speeds to 6000 rpm.

The flow of air into the engine was measured using a laminar flow element (Meriam Model No. 25 MC2). The flow element was separated from the engine by a plenum chamber which dampened pulsations from the intake strokes of the engine so that air flow through the laminar element would be relatively steady.

Fuel flow was measured by a Flotron positive displacement type flow metering system.

The engine coolant was a one-to-one volume solution of ethylene glycol and water. The coolant flow was measured by a turbine flowmeter. Both the inlet and outlet coolant temperatures along with exhaust temperature and housing temperature were monitored. These were used to determine the establishment of steady state operation at a predefined engine speed.

Pressures in the combustion chamber of the engine were measured by a series of four water cooled, AVL piezoelectric pressure transducers. These transducers were mounted in the midplane of the trochoid housing in such a way that the pressure in a chamber of interest would constantly be monitored (fig. 4). Pressure monitoring throughout the four-stroke cycle was made possible through the use of a NASA developed electronic switching and correlating system called the Modular Equipment Instrument System (MEIS) (ref. 6). The MEIS correlates the individual pressure signals into one composite curve of pressure as a function of engine crank angle for each complete four-stroke engine cycle. The crankshaft position was provided to the MEIS by an optical encoder (Renco Corp. Model No. 30HDAE-N8) with a resolution of 0.53°.

This composite pressure curve, which is a real-time measurement, was recorded on a digital waveform recorder. The waveform recorder incorporated a

series of individual analog-to-digital (A-D) converters which permitted a number of individual signals to be recorded simultaneously (fig. 5). The commercially available wave form recorder (Gould 9000 Series) was modified such that it could be triggered externally with sampling also controlled externally. The recorder was triggered manually when a steady state condition was reached with the engine. The recording was done in a crank angle reference frame as opposed to a time-base reference frame. The external clock signal and trigger were produced by a NASA designed MEIS/waveform recorder interface module.

The individual composite pressure curves stored 1080° of crankshaft rotation in 1024 address locations. There were 256 b (± 128 b) of vertical resolution per channel. This presented some problems in accurate data collection and in further analysis where small pressure changes yielded poor data resolution. Each A-D converter had 32 KB of memory associated with it, which translates into 32 composite pressure curves. For each data point taken, 32 consecutive composite curves were recorded and automatically down loaded to a microcomputer having hard-disk memory capability. These 32 composite curves were ensemble-averaged in post-run time to form one average composite pressure curve representative of the engine conditions at the time data was taken.

RESULTS AND DISCUSSION

Results of Heat Release Analysis

Figure 6 shows the comparison of several computed and experimental pressure profiles corresponding to different values of engine speeds and loads. Agreements between the predicted and experimental ensembled pressure profiles, peak pressures, and crank angles at peak pressure are good.

Results for the combustion heat release rates at brake mean effective pressures (BMEP's) of 138.5, 137.3, 142.9, 139.3, 164.0, 163.5, 113.3, and 102.4 kPa are presented in figure 7. The rate of combustion heat release was plotted against crank angle for several speed and load conditions. Each curve is calculated using an average of 32 consecutive cycles of the experimental pressure data. The general trend of these figures shows an increase in the value of the peak rate, hence an improvement in the combustion efficiency, as BMEP increases at each engine speed. The oscillations observed at the peak rate of heat release at 137.3 kPa BMEP indicate that the accuracies of the heat release analysis rely on the accuracies of the experimental pressure data. The heat release analysis uses the derivative of the chamber pressure, hence smooth and highly resolved pressure data are necessary to obtain accurate heat release rate results. Experimental pressure data analyzed with the heat release rate program should also be ensemble averaged over a large number of carefully measured single cycle pressure data so that the effects of cycle to cycle variations are not overly weighted.

All the heat release rate curves exhibit two stages of combustion. The first stage of combustion starts at about 525 and ends at approximately 560 crank angle degrees after BDC or minimum volume on the cool side of the engine. The second stage starts at the end of the first stage and proceeds into the expansion stroke. It should be noted that the heat release rate results during the second stage are sensitive to the inaccuracies in the pressure data. As mentioned in the previous section, the pressure data digitized by the 8 b A-D converter does not have adequate resolution in the lower pressure range. For

example, if the maximum pressure in the chamber is 500 psi, then the incremental pressure change is $500 \text{ psi}/(2^8/2) = 3.91 \text{ psi}$. At peak pressure the error is $3.91/500 = 0.8$ percent, but near the intake and exhaust the error is $3.91/14.7 = 26.6$ percent. Thus for the better pressure resolution, a 10 b or higher A/D convertor would be more suitable. A problem is also created by the digital recorder when the heat release rate, $dQ/d\theta$, is derived from the empirical pressure curve. At regions in the engine cycle where the rate of pressure change is relatively slow, the digital equipment cannot record a curve that is differentiable.

A complete understanding of the combustion process would require detailed modeling of the compressible viscous air motion, fuel spray penetration, droplet break-up and evaporation, air entrainment into the spray, turbulent diffusion, combustion kinetics, and so on. The description by Watson et al (ref. 7) of different stages of Diesel combustion may be used here to explain the two stages of combustion observed in DISC Wankel engines. Watson et al proposed that the apparent fuel burning rate in Diesel engines could be expressed as the sum of two components, one relating to premixed (Stage 1) and the other to diffusion-controlled burning (Stage 2). In Stage 1, combustion of the fuel which has already mixed with air to within the flammability limits occurs fairly rapidly. Once the premixed fuel and air mixture has been consumed, combustion in stage two is controlled by the lower rate at which the fuel air mixture becomes available for diffusion burning. The second stage of combustion continues well into the expansion stroke and eventually would asymptotically approach zero.

A typical integrated heat release rate is presented in figure 8. The integrated heat release rate indicates that roughly half of the fuel is burned in the first stage. The majority of the remaining fuel is burned in the second stage. Less than 5 percent of the fuel consists of unburned hydrocarbons which are swept through the exhaust system. Performance loss mechanisms are shown in the integrated heat release rate presented in figure 8. The lowest, curve 1, is the net heat release; it represents the net thermal efficiency and the sensible internal energy changes of the charge. The next, curve 2, shows the effect of adding heat transfer to engine structures. The next, curve 3, shows the gross heat release which combines the effects of adding heat transfer, crevice volume and leakage area. This is the computed gross heat release curve which represents the amount of chemical energy which is released as thermal energy by combustion. The straight line along the top of figure 8 represents the fuel chemical energy within the chamber, i.e., the mass of fuel in the chamber times the lower heating value per unit mass. The difference between this straight line and the gross heat release curve gives a rough estimate of the combustion inefficiency. The breakdown of these loss mechanisms at various speeds and loads for the OMC rotary test engine is given in table II.

To complete the formulation of the combustion model, a single heat release rate curve (fig. 9) was generated by averaging the rates shown on figure 7. It was decided to exclude the rate data at low speed (2200 rpm) since poor combustion efficiency was demonstrated at these operating points (low peak values of heat release rates at 2200 rpm as shown on fig. 7). As a first attempt, the empirical model described in the previous section was used to represent the rate of heat release in the engine simulation. Figure 9 shows the comparison of the average heat release rate with results from the best-fitted empirical model. Model parameter values for the results shown in figure 9 were:

$$\theta_s = 12^\circ \text{ BIC}$$

$$\theta_m = 6.5^\circ \text{ AIC}$$

$$(dQ/d\theta)_m = 0.028 \text{ (1/deg)}$$

$$\tau = 26.107^\circ$$

The calibration of the submodels of heat release, heat transfer, leakage, crevice effects, etc. also resulted in the value of other parameters in the OMC rotary test engine simulation model as follows:

Heat transfer constants: $C_1 = 0.0625$; $C_2 = 0.163$

Leakage area per apex: 0.02 cm^2

Crevice volume: 0.875 cm^3

Discharge coefficients: 0.6 (intake), 0.6 (exhaust)

Estimated temperatures of the rotor face and measured temperatures of the side and rotor housing surfaces at various operating conditions were used in the simulation. The effects of various operational parameters on the performance of the OMC engine were analyzed by the DISC Wankel simulation model and its predicted results are discussed next.

Engine Performance Results

Calculations were carried out for the engine over a speed range from 2200 to 3200 rpm at mid and light load. The simulation output was checked against performance test data. The various calculated parameters, i.e., volumetric efficiency, power output, indicated specific fuel consumption (ISFC) and exhaust temperature are presented in figures 10 and 11. Only indicated performance of the OMC Wankel engine was predicted since the DISC Wankel simulation model includes no friction.

Figure 10 shows the comparison of the indicated values of the power output and specific fuel consumption predicted by the simulation with experimental values of the brake horsepower and brake specific fuel consumption, respectively, at varying speeds. There is good agreement in the trend of indicated power output from the simulation and the brake horsepower from the engine data. The brake horsepower test data values are about 20 percent lower than the indicated horsepower values from the simulation. Reasonable agreement also exists in the trend of the indicated specific fuel consumption from the simulation and the test data brake specific fuel consumption over the speed range with the exception of the data at the speed of 3200 rpm. The predicted indicated specific fuel consumption values fall about 1.5 times below the experimental brake specific fuel consumption. Over the speed and load range studied, the predicted maximum indicated power output developed at 7.14 hp at 3200 rpm and $\phi = 0.39$. The predicted minimum ISFC of 294 g/kW-hr was also obtained at the same speed and load condition.

Figure 11 shows the comparison of the volumetric efficiency and exhaust temperature values predicted by the simulation with the engine data. Comparison of the values for volumetric efficiency show differences varying from 0 to 18 percent. The trends in the predicted exhaust temperature values closely match the experimental trends. It should be noted that the lower exhaust tem-

perature values from engine data is due to coolant circulating around the exhaust port of the test engine.

The effects of changes in the combustion rate, turbocharging and leakage area on performance characteristics of the OMC rotary test engine were studied by the DISC Wankel simulation model and the results are discussed next. Tests were carried out for the following reference condition: 3200 rpm, $\phi = 0.39$. To make these parametric studies, one parameter was changed at a time while the other parameters were kept at the reference condition.

The Effect of Combustion Rate

Understanding the combustion process plays an important role in the optimization of engine performance and efficiency. To change the combustion rate in the OMC engine simulation, the combustion duration was adjusted. The combustion duration is defined as the crank angle interval from 10 percent mass fraction burned to 90 percent mass fraction burned. The crank angle interval between the actual spark timing and 10 percent mass fraction burned defines the ignition delay period. Thus a change in the combustion duration was induced by a change in the spark timing, which is specified as an input.

The simulation model predicts a significant improvement in the OMC rotary engine performance with an increase in the combustion rate. Figures 12(a) to (d) present the effect of combustion duration on the mass fraction burned profile, chamber pressure and temperature profiles, and power output for the naturally aspirated OMC engine (3200 rpm, compression ratio CR = 12.94). The value of the spark timing was varied from -22° to 6° BTC. The normalized mass fractions burned at three different burn durations (54° , 61° and 67° crank angle) are shown in figure 12(a). The curve indicates an improvement in the shape of burned fraction at the shorter combustion durations because more of the fuel is burned earlier in the cycle. The simulation model also predicts a significant increase in the peak pressure with faster combustion. The chamber temperature near top-dead-center is also seen to increase for 54° and 61° crank angle burn duration. The total work output per cycle from the P-V diagrams shown in figure 12 increases with faster combustion.

Figure 13 presents the effect of combustion duration on the power output, indicated mean effective pressure (IMEP), ISFC and exhaust temperature for the OMC engine (3200 rpm, CR = 12.94). The model predicts a significant increase in power output and IMEP with faster combustion. The model also predicts a significant decrease in ISFC and exhaust temperature with faster combustion.

The Effect of Leakage Area

Leakage past the apex and side seals is an important source of performance loss in the Wankel rotary engine. Eberbe and Klomp (ref. 8) predicted that a reduction in the leakage area of 5 percent at 2000 rpm will reduce ISFC by 6.5 percent. The side seal spring modifications made by Yamamoto and Muroki (ref. 9) reduce brake specific fuel consumption by 3.5 percent at 1500 rpm over a load range of 1.5 to 4 kg/cm² BMEP.

The model used in this study combines apex and side seal leakage into three apex seal leakage areas. Figure 14 shows the effect of reduced leakage

area on the ISFC, exhaust temperature, power output and volumetric efficiency for the OMC rotary engine (3200 rpm, CR = 12.94). The model predicts a significant improvement in the OMC rotary engine performance with reduced leakage. As the leakage area is reduced from 0.02 to 0.005 cm² per apex, the following improvements are observed: power is increased by 40 percent, exhaust temperature is increased by 6.4 percent, volumetric efficiency is increased by 11 percent and ISFC is decreased by 45 percent. Although a 75 percent decrease in leakage is not easily accomplished, even modest reductions in leakage will result in significant performance improvements.

The Effect of Turbocharging

Figure 15 shows the effect of turbocharging the OMC rotary engine at 3200 rpm and CR = 12.94. These results indicate a significant improvement in performance over the naturally aspirated engine. An increase in power output of 78.5 percent is observed as the intake pressure is increased by 31 percent. An increase in the intake pressure by the same amount also increases the exhaust temperature by 32.5 percent. Significant increases in IMEP, peak pressure and volumetric efficiency are also observed as the intake/exhaust pressure ratio is increased.

CONCLUSIONS

The Outboard Marine Corporation (OMC) single rotor test engine has been set up at NASA Lewis to carry out experimental investigations on the stratified-charge concept. Computer models of the heat release rate and engine simulation of the DISC Wankel engine system have been used to study the engine performance loss mechanisms and to investigate how the performance of the DISC Wankel engine varies with changes in engine design and operating conditions. Comparison of calculation results with experimental data was provided and the major conclusions which have been drawn from this study are:

1. Combustion in the OMC engine displays two stages. Stage one of combustion occurs rapidly. This rapid, premixed combustion period begins about 525 and ends approximately 560 crank angle degrees after BDC. The premixed combustion process is then followed by the second stage (diffusion burning) which occurs more slowly and continues well into the expansion stroke.
2. Carefully measured pressure data that are ensemble averaged over a large number of single cycles are required for an accurate heat release analysis.
3. Good agreement in chamber pressure profiles and performance results over the range of speeds and loads examined indicates that the combination of heat release rate and engine simulation models provide an effective means of predicting engine performance and loss mechanisms. Thus, the heat release analysis and engine simulation model provide fast and simple yet powerful and practical approaches to assist in understanding the stratified charge combustion process. In addition, by simulating changes in engine design and operating conditions the engine simulation model can accurately predict the performance of a DISC Wankel engine.

4. The engine simulation model predicts a significant improvement in the performance of the Wankel engine performance with faster combustion, reduced leakage and turbocharging. The need for faster combustion, reduced leakage and turbocharging is quite apparent from these results.

ACKNOWLEDGMENT

H. L. Nguyen thanks Professor J. B. Heywood for several helpful discussions. We thank Dr. H. J. Schock for his critique of the manuscript.

REFERENCES

1. E.A. Willis, and W.T. Wintucky, "An Overview of NASA Intermittent Combustion Engine Research," AIAA Paper 84-1393, June 1984.
2. R.E. Mount, A.E. Parunte, and W.F. Hady, "Stratified-Charge Rotary Engine for General Aviation," ASME Paper 86-GT-181, June 1986.
3. J.A. Roberts, T.J. Norman, J.A. Ekchian, and J.B. Heywood, "Computer Models for Evaluating Premixed and DISC Wankel Engine Performance," SAE Paper 860613, Feb. 1986.
4. J.A. Gatowski, E.N. Balles, K.M. Chun, F.E. Nelson, J.A. Ekchian, and J.B. Heywood, "Heat Release Analysis of Engine Pressure Data," SAE Paper 841359, 1984.
5. G. Woschni, "A Universally Applicable Equation for the Instantaneous Heat Transfer Coefficient in the Internal Combustion Engine," SAE Paper 670931, 1967.
6. H.J. Schock, W.J. Rice, and P.R. Meng, "Experimental Analysis of IMEP in a Rotary Combustion Engine," SAE Paper 810150, 1981.
7. N. Watson, A.D. Pilley, and M. Marzouk, "A Combustion Correlation for Diesel Engine Simulation," Diesel Combustion and Emissions, SAE P-86, 1980, pp. 51-64.
8. M.K. Eberle, and E.D. Klomp, "An Evaluation of the Potential Performance Gain for Leakage Reduction in Rotary Engines," SAE Paper 730117, 1973.
9. K. Yamamoto, and T. Muroki, "Development of Exhaust Emissions and Fuel Economy of the Rotary Engine at Toyo Kogyo," SAE Paper 780417, 1978.

TABLE I. - ENGINE SPECIFICATIONS OMC DISC SINGLE ROTOR TEST ENGINE

Displacement	648 cc (39.6 cu. in.)/rotor face
Compression ratio	12.94
Eccentricity (e)	15.0 mm (.5906 in.)
Generating radius (R)	103.5 mm (4.0748 in.)
Oversize (a)	1.5 mm (0.0591 in.)
Trochoid width (W)	79.2 mm (3.118 in.)
Port timings (degree)	
Exhaust port opens at	-630
Exhaust port closes at	-226
Intake port opens at	196
Intake port closes at	585
Fuel:	
ASTM Diesel High Cetane Check Fuel	
Cetane No.	53.7
Gross heat value	19,655 Btu/lb (45,723 kJ/kg)

TABLE II. - RESULTS OF HEAT RELEASE ANALYSIS OF OMC WANKEL ROTARY ENGINE AT VARIOUS SPEEDS AND LOADS

[Expressed as Percent of Introduced Fuel Chemical Energy.^a]

	Percent thermal efficiency plus percent change in sensible internal energy	Percent heat transfer to structures	Percent heat loss to crevice volume and leakage area
3200 rpm ø = 0.39	61	34.0	3.0
3200 rpm ø = 0.34	60	36.2	2.7
2800 rpm ø = 0.410	52.5	39.5	4.8
2800 rpm ø = 0.34	58	35.0	4.2
2500 rpm ø = 0.43	50.5	40.7	5.4
2500 rpm ø = 0.41	45	47.2	5.4
2200 rpm ø = 0.37	36	55.8	5.3
2200 rpm ø = 0.34	58.5	33.2	5.3

^aIn each case, the unaccounted percent fuel energy is a rough estimate of the combustion inefficiency.

ORIGINAL PAGE IS
OF POOR QUALITY

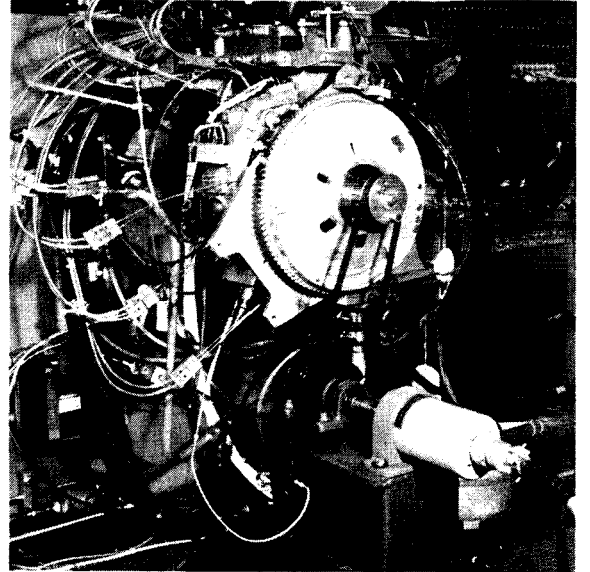
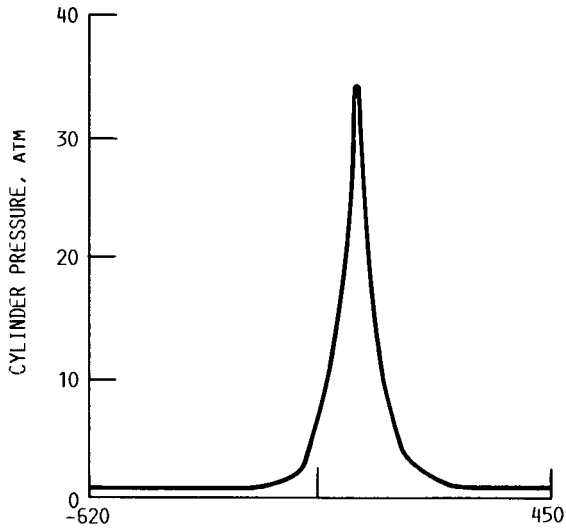


FIGURE 2. - INSTRUMENTED OMC WANKEL ROTARY ENGINE.

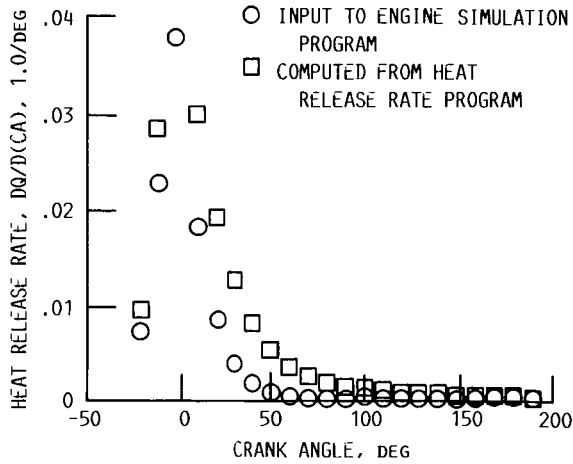


FIGURE 1. - PREDICTED CYLINDER PRESSURE FROM ENGINE SIMULATION USED TO TEST HEAT RELEASE RATE PROGRAM, AND COMBUSTION HEAT RELEASE RATES FOR OMC WANKEL ROTARY ENGINE. SPEED, 3200 RPM; EQUIVALENCE RATIO, 0.39.

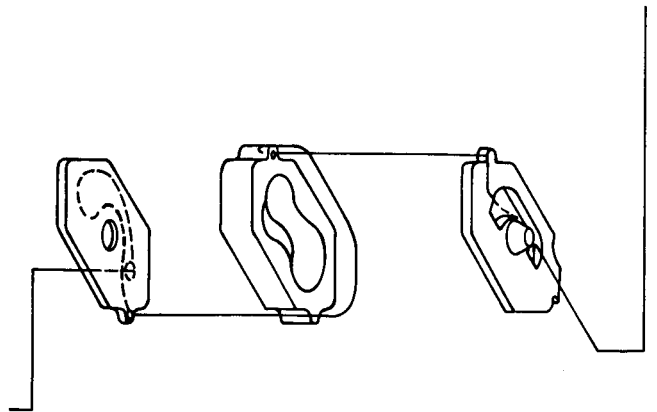


FIGURE 3. - COOLANT FLOW THROUGH ENGINE.

ORIGINAL PAGE IS
OF POOR QUALITY

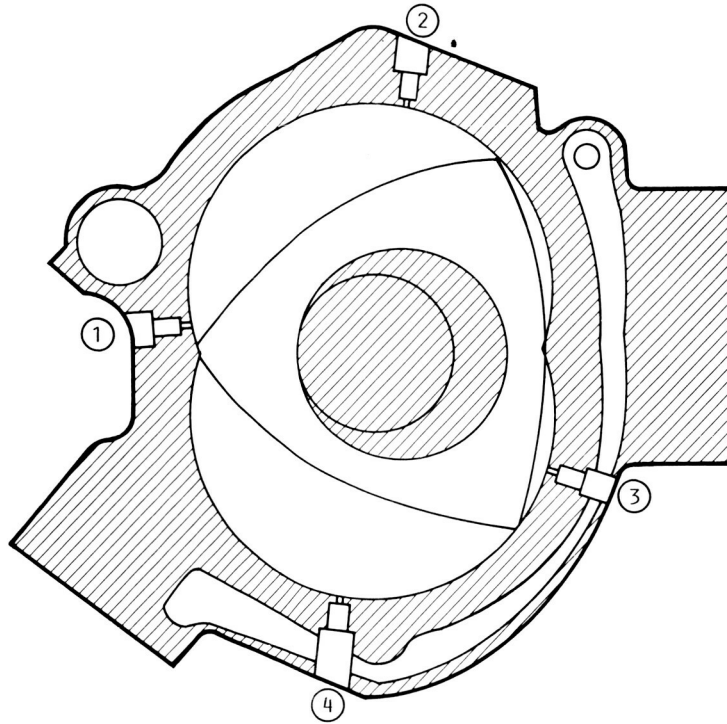


FIGURE 4. - PRESSURE TRANSDUCER LOCATIONS.

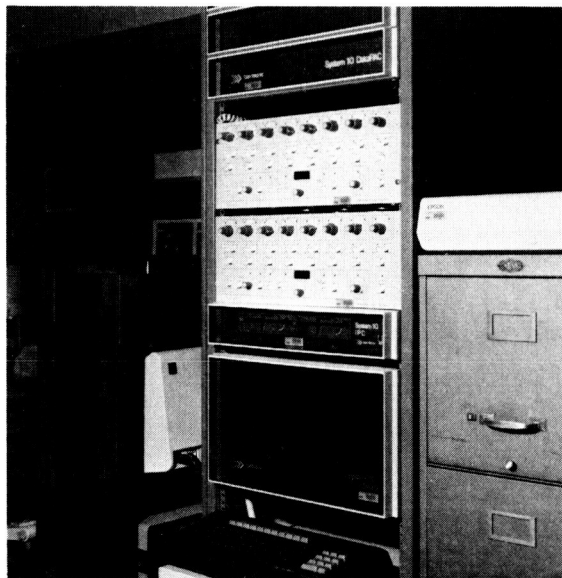
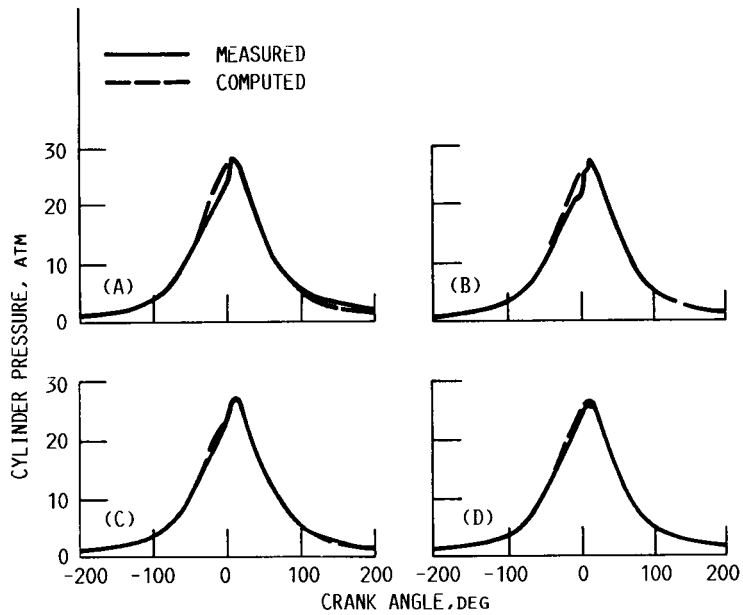
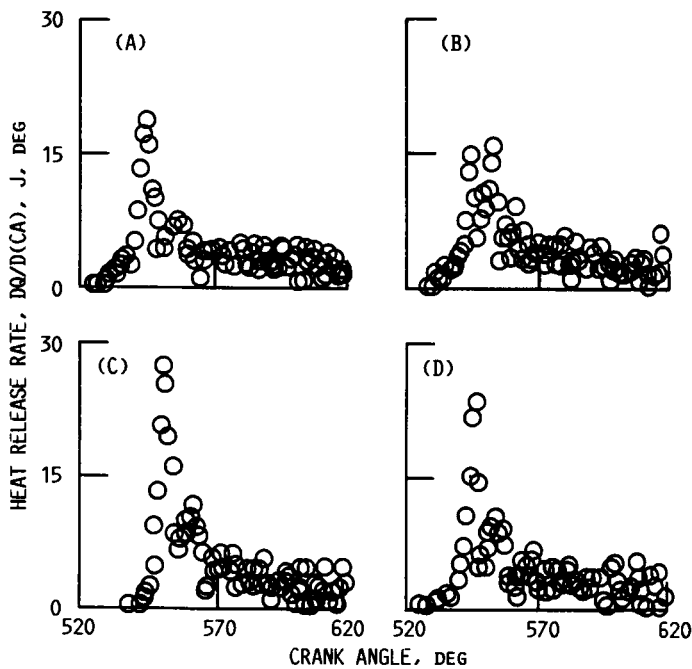


FIGURE 5. - A-D REAL TIME DATA RECORDING SYSTEM.



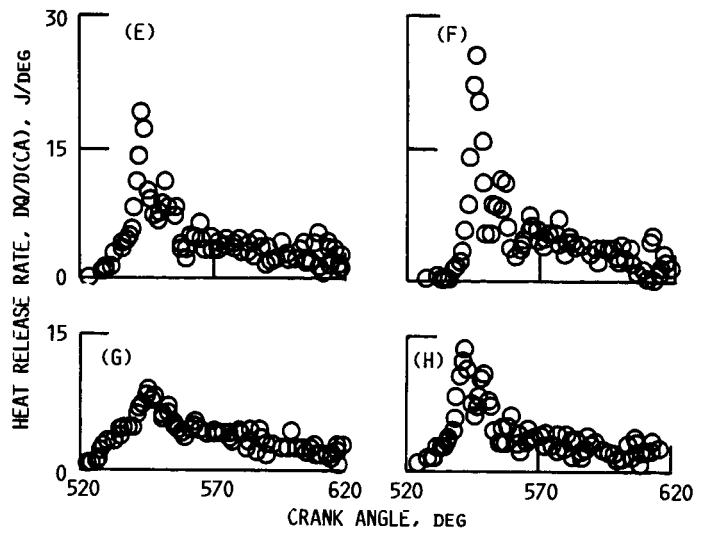
(A) SPEED, 3200 RPM; (B) SPEED, 2800 RPM;
 EQUIVALENCE RATIO, 0.39. EQUIVALENCE, 0.41.
 (C) SPEED, 2500 RPM; (D) SPEED, 2200 RPM;
 EQUIVALENCE RATIO, 0.427. EQUIVALENCE RATIO, 0.37.

FIGURE 6. - MEASURED AND PREDUCTED CYLINDER PRESSURES FOR OMC WANKEL ROTARY ENGINE AT VARIOUS SPEEDS AND LOADS.



(A) SPEED, 3200 RPM; EQUIVALENCE RATIO, 0.39;
 BMEP, 138.5 kPA.
 (B) SPEED, 3200 RPM; EQUIVALENCE RATIO, 0.34;
 BMEP, 137.3 kPA.
 (C) SPEED, 2800 RPM; EQUIVALENCE RATIO, 0.338;
 BMEP, 142.9 kPA.
 (D) SPEED, 2800 RPM; EQUIVALENCE RATIO, 0.41;
 BMEP, 139.3 kPA.

FIGURE 7. - COMBUSTION HEAT RELEASE RATE FOR OMC WANKEL ROTARY ENGINE AS FUNCTION OF CRANK ANGLE AT VARIOUS SPEEDS, LOADS, AND BRAKE MEAN EFFECTIVE PRESSURE (BMEP).



(E) SPEED, 2500 RPM; EQUIVALENCE RATIO, 0.41;
 BMEP, 164.0.
 (F) SPEED, 2500 RPM; EQUIVALENCE RATIO, 0.427;
 BMEP, 163.5.
 (G) SPEED, 2200 RPM; EQUIVALENCE RATIO, 0.37;
 BMEP, 113.3.
 (D) SPEED, 2200 RPM; EQUIVALENCE RATIO, 0.39;
 BMEP, 102.4 kPA.

FIGURE 7. - CONCLUDED.

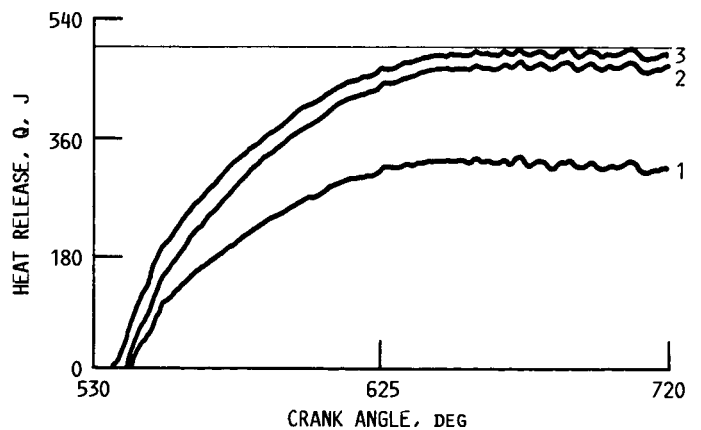


FIGURE 8. - INTEGRATED COMBUSTION HEAT RELEASE FOR OMC WANKEL ROTARY ENGINE AS FUNCTION OF CRANK ANGLE. SPEED, 2200 RPM; EQUIVALENCE RATIO, 0.34; BRAKE MEAN EFFECTIVE PRESSURE, 113.3 kPA.

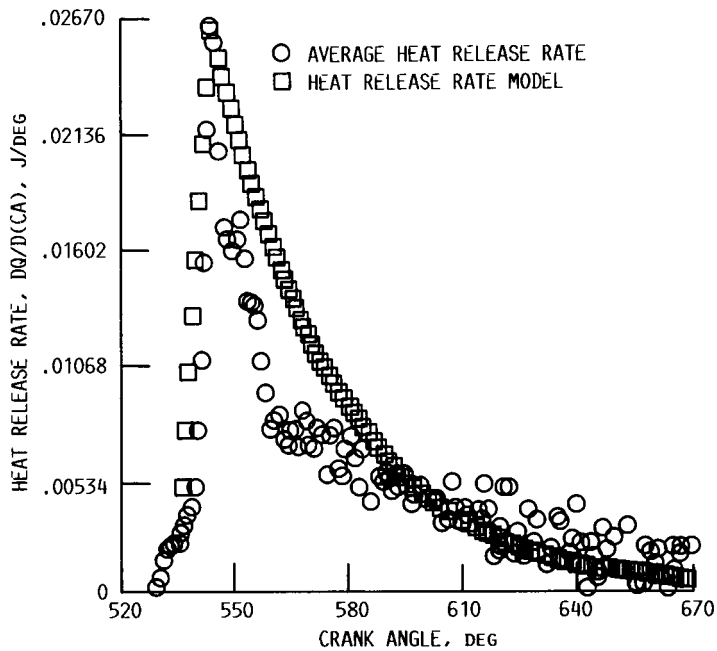


FIGURE 9. - AVERAGE HEAT RELEASE RATE AND EMPIRICAL HEAT RELEASE RATE MODEL AS FUNCTIONS OF CRANK ANGLE.

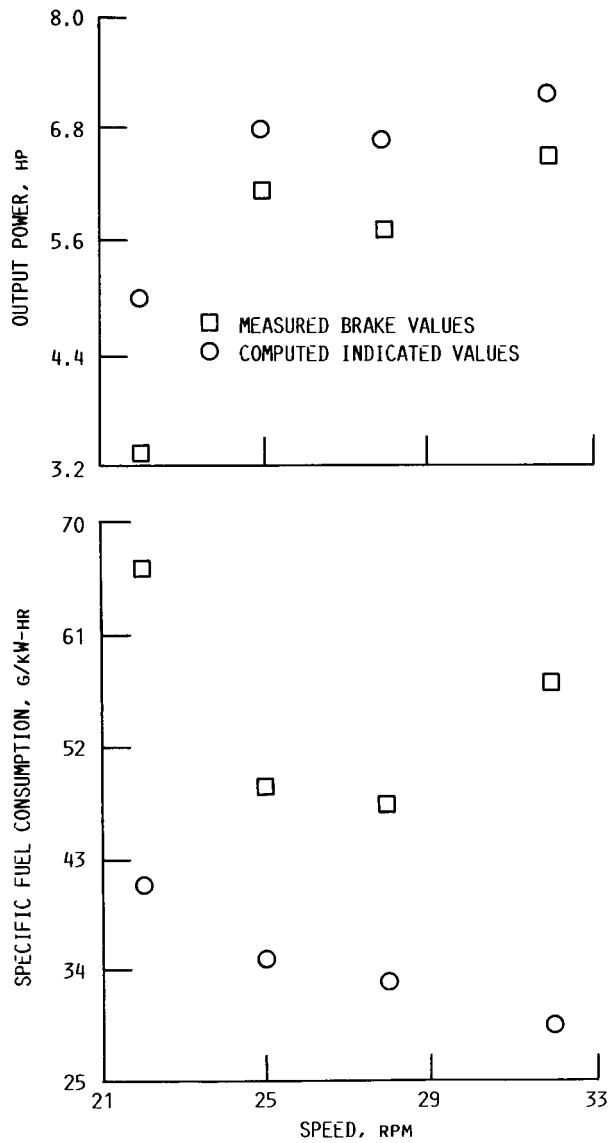


FIGURE 10. - INDICATED VALUES OF OUTPUT POWER AND SPECIFIC FUEL CONSUMPTION FOR OMC WANKLE ROTARY ENGINE PREDICTED BY SIMULATION WITH THEIR RESPECTIVE EXPERIMENTAL VALUES.

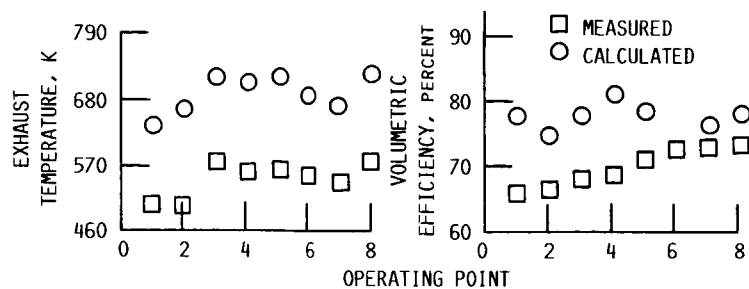


FIGURE 11. - MEASURED AND PREDICTED EXHAUST TEMPERATURE AND VOLUMETRIC EFFICIENCY FOR OMC WANKEL ROTARY ENGINE AT VARYING SPEEDS AND EQUIVALENCE RATIO ϕ . THE OPERATING POINTS LABELED ON X-AXIS ARE 1 = (2200 RPM, $\phi = 0.34$), 2 = (2200 RPM, $\phi = 0.37$), 3 = (2500 RPM, $\phi = 0.43$), 4 = (2500 RPM, $\phi = 0.41$), 5 = (2800 RPM, $\phi = 0.41$), 6 = (3200 RPM, $\phi = 0.34$), 7 = (2800 RPM, $\phi = 0.34$), 8 = (3200 RPM, $\phi = 0.39$).

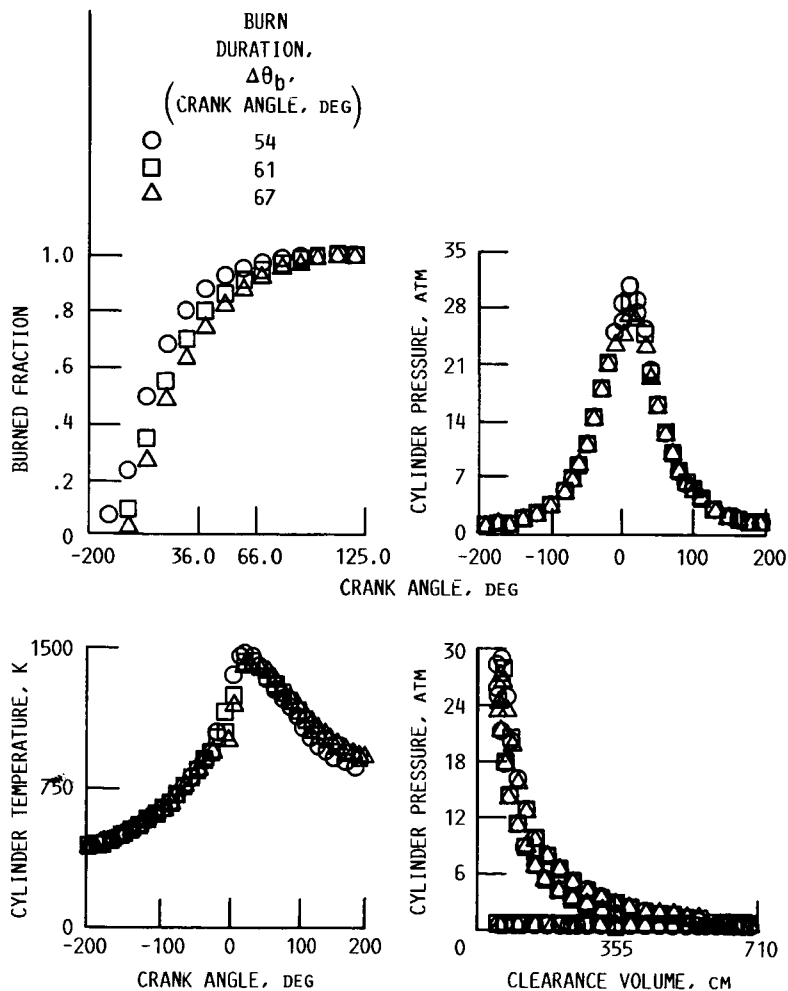


FIGURE 12. - MASS BURNED FRACTION, CYLINDER PRESSURE, CYLINDER TEMPERATURE, AND POWER OUTPUT OF OMC WANKEL ROTARY ENGINE AS FUNCTIONS OF BURN DURATION. SPEED, 3200 RPM; EQUIVALENCE RATIO, 0.39.

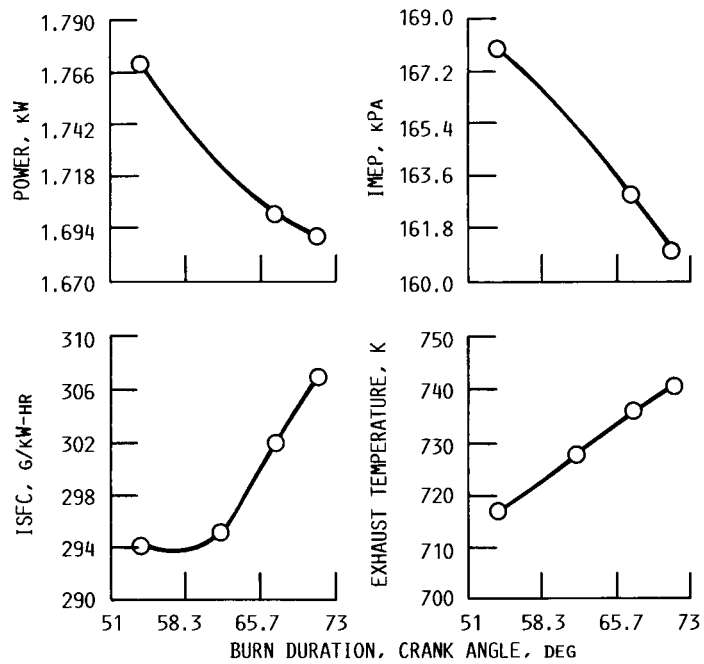


FIGURE 13. - EFFECT OF COMBUSTION DURATION ON THE POWER OUTPUT, IMEP, ISFC AND EXHAUST TEMPERATURE OF THE OMC WANKEL ROTARY ENGINE AT 3200 REV/MIN, $\Phi = 0.39$.

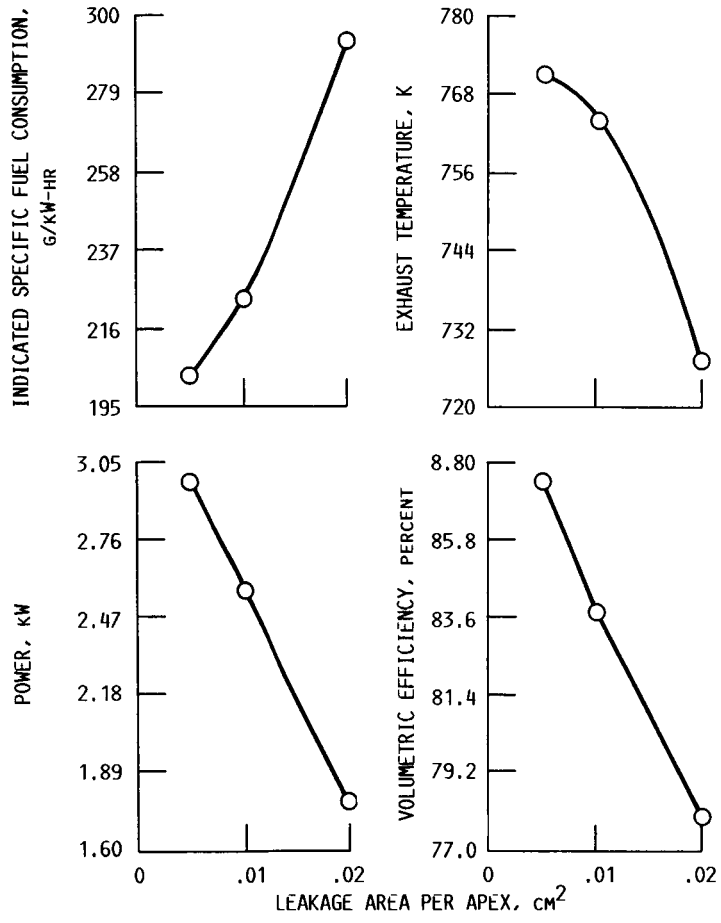


FIGURE 14. - INDICATED SPECIFIC FUEL CONSUMPTION, EXHAUST TEMPERATURE, POWER OUTPUT, AND VOLUMETRIC EFFICIENCY OF OMC WANKEL ROTARY ENGINE AS FUNCTIONS OF LEAKAGE AREA PER APEX. SPEED, 3200 RPM; EQUIVALENCE RATIO, 0.39.

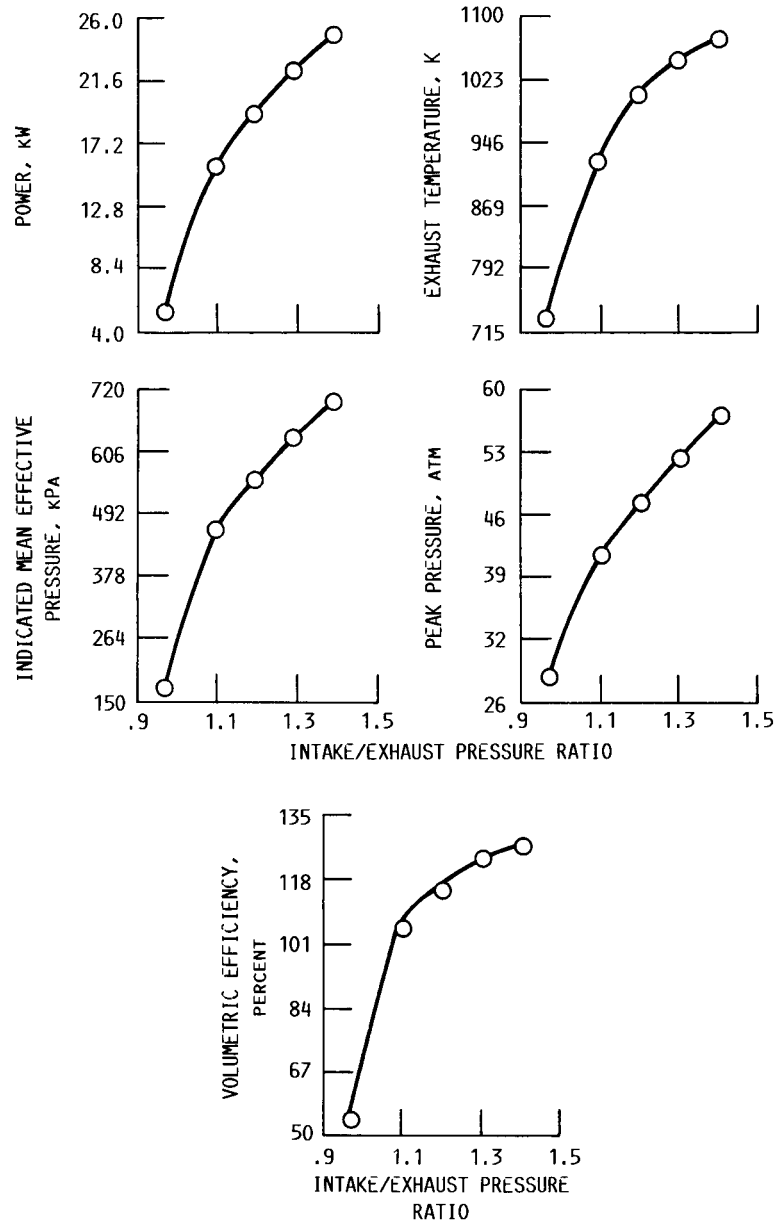


FIGURE 15. - POWER OUTPUT, EXHAUST TEMPERATURE, INDICATED MEAN EFFECTIVE PRESSURE, PEAK PRESSURE, AND VOLUMETRIC EFFICIENCY OF OMC WANKEL ROTARY ENGINE AS FUNCTIONS OF INTAKE/EXHAUST PRESSURE RATIO (TURBOCHARGING). SPEED, 3200 RPM; EQUIVALENCE RATIO, 0.39.

1. Report No. NASA TM-89833		2. Government Accession No.		3. Recipient's Catalog No.	
4. Title and Subtitle Performance and Efficiency Evaluation and Heat Release Study of an Outboard Marine Corporation Rotary Combustion Engine				5. Report Date April 1987	
				6. Performing Organization Code 505-62-11	
7. Author(s) H.L. Nguyen, H.E. Addy, T.H. Bond, C.M. Lee, and K.S. Chun				8. Performing Organization Report No. E-3488	
				10. Work Unit No.	
9. Performing Organization Name and Address National Aeronautics and Space Administration Lewis Research Center Cleveland, Ohio 44135				11. Contract or Grant No.	
				13. Type of Report and Period Covered Technical Memorandum	
12. Sponsoring Agency Name and Address National Aeronautics and Space Administration Washington, D.C. 20546				14. Sponsoring Agency Code	
15. Supplementary Notes Prepared for the 1987 International Congress and Exposition, sponsored by the Society of Automotive Engineers, Detroit, Michigan, February 23-27, 1987.					
16. Abstract A computer simulation which models engine performance of Direct Injection Stratified Charge (DISC) rotary engines has been used to study the effect of variations in engine design and operating parameters on engine performance and efficiency of an experimental Outboard Marine Corporation (OMC) rotary combustion engine. Engine pressure data have been used in a heat release analysis to study the effects of heat transfer, leakage and crevice flows. Predicted engine data is compared with experimental test data over a range of engine speeds and loads. An examination of methods to improve the performance of the rotary engine using advanced heat engine concepts such as faster combustion, reduced leakage and turbocharging is also presented.					
17. Key Words (Suggested by Author(s)) Performance; Efficiency; Heat release; Direct-injection stratified-charge rotary engine			18. Distribution Statement Unclassified - unlimited STAR Category 07		
19. Security Classif. (of this report) Unclassified		20. Security Classif. (of this page) Unclassified		21. No. of pages 22	22. Price* A02